Quantum Tomography of Nonclassical Light

S. F. Pereira, G. Breitenbach, S. Schiller, and J. Mlynek

Fakultät für Physik, Universität Konstanz, D-78434 Konstanz, Germany
Phone: +49(7531) 883842, FAX +49(7531) 883072, gerdb@spock.physik.uni-konstanz.de
to appear in Proc. of the 1995 Les Houches School on "Quantum Fluctuations", S. Reynaud and E. Giacobino, eds.

1 Introduction

Over the years, research in quantum optics has been increasingly progressing both theoretically and experimentally, with successful tests and demonstrations of quantum theory. Among relatively simple but rather rich systems used in quantum optics experiments, the proccess of parametric down-conversion of light has been vastly explored. Several systems involving this phenomenon have been used as tools in experiments investigating fundamental principles of quantum mechanics such as the violation of Bell's inequalities,[1] the Einstein-Podolsky-Rosen paradox,[2] the demonstration of the Heisenberg uncertainty principle,[3] and quantum nondemolition measurements.[4] Particularly interesting is the generation of squeezed vacuum states through the parametric down-conversion process. These states have the property that the quantum noise is redistributed over the quadrature amplitudes of the field. This redistribution is such that for a particular choice of the measured quadrature, the noise is less than that of the vacuum state. By using the squeezed vacuum state as an input to other systems, several achievements in the area of precision measurements have been realized, such as sub-shot noise interferometry and atomic spectroscopy,[5, 6] noise reduction in optical amplification,[7] quantum duplication,[8] and improved back-action evasion measurements.[9]

In these experiments, an essential question is how to measure such small fluctuations with a good degree of accuracy. A technique that has been widely used to determine the degree of nonclassicality, i.e. the level of fluctuations with respect to the vacuum fluctuations, is balanced homodyne detection.[10] This is a very reliable and sensitive device, where the quantum field is mixed with a strong light beam, usually referred to as the local oscillator, at a beamsplitter. The two outputs of the beamsplitter are detected and their respective photocurrents subtracted. It can be shown that the resulting photocurrent is proportional to the quadrature field amplitude of the quantum field only, the fluctuations of the local oscillator being suppressed to a large extent. Since the measured photocurrent relates to the quadrature field amplitude of one port of the beamsplitter only (i.e., the port where the quantum field is injected), the reference level in this type of measurement is determined by simply blocking the quantum field, thus accessing the vacuum fluctuations. Another particular feature of homodyne detection is that by changing the phase of the local oscillator with respect to that of the quantum field, one is able to determine not only the fluctuations of the amplitude ($\hat{x}$) or phase ($\hat{p}$) quadratures of the field, but also of any linear combination $\hat{x}_\theta = \hat{x}\cos\theta + \hat{p}\sin\theta$, where $\hat{x} = 2^{-1/2}(\hat{a} + \hat{a}^\dagger)$ and $\hat{p} = -2^{-1/2}i(\hat{a} - \hat{a}^\dagger)$, and $\hat{a}$, $\hat{a}^\dagger$ are the annihilation and creation operators.

So far, most of the squeezing experiments reported in the literature are restricted to the measurement of the variances of the quadratures amplitudes. Although such information is enough to determine, for example, the degree of squeezing, it has been discovered recently that complete information about the quantum field can be obtained by measuring $P_\theta(x_\theta)$, the probability distribution functions for x_θ for a large number of phase angles θ. This set of distributions allows to reconstruct both the Wigner function and the density matrix of the quantum field.[11]-[15] This possibility opened a new prospective in measurements of quantum fields. For example, the photon number distribution of states, in particular of squeezed vacuum, can be obtained without photon counting techniques, which are more complicated and sometimes not possible because of the low counting efficiencies in the near infrared region.[16] Apart from the experimental achievement per se, the knowledge of the Wigner function and of the density matrix mean a complete characterization of a quantum state. This technique, now being applied to rather well-understood optical states, may in future be used to fully characterize "unknown" quantum states.

The generation of a squeezed vacuum state together with its complete characterization via the determination of the density matrix is the subject of this paper. In addition, we have also directed our efforts to build a simple, compact and stable source of squeezed light with the use of a monolithic resonator,[17] which may in future contribute to bridge the gap between demonstrations and real applications of squeezed light.

The paper is organized as follows. In Section 2, we present a detailed explanation of the experimental set-up and the procedure for the measurements. In section 3, the measurements of squeezing are shown, which include the squeezing spectrum, the squeezing at a fixed frequency, and the distribution functions for various field quadratures. Section 4 is devoted to the reconstruction of the Wigner function, the photon number distribution and the density matrix of the squeezed vacuum state. The conclusions are presented in Section 5.

2 Generation of Squeezed Light

The squeezed vacuum state is generated via degenerate nonlinear frequency down-conversion of a pump light field. This implies the use of a nonlinear crystal, pumped by a frequency 2ω, in which the conversion process $2\omega \rightarrow \omega + \omega$ occurs, leading to parametric amplification/deamplification of the quadratures of the ω-mode. Since the conversion efficiency for this process is usually small, two alternate approaches are commonly employed: the use of optical cavities that enhance the gain of the parametric amplification for at a given pump power,[3, 6, 18] or single pass down-conversion with high peak power pump pulses.[12, 19]

In the work presented here, the parametric amplification occurs in a monolithic resonator pumped below its threshold of oscillation. Thus, the basic elements of the experiment are a main laser source, a frequency doubler, the optical parametric oscillator (OPO), and the detection system. The general idea of the experiment consists in first frequency doubling most of the laser power to the frequency 2ω. This wave subsequently pumps the OPO. The output field of the OPO is then mixed with a local oscillator for balanced homodyne detection (BHD). The choice of first frequency doubling and then down-converting the light is very practical since a small fraction of the laser power can be picked off for use as a reliable local oscillator for the BHD. In addition to having the same frequency as the squeezed light, the use of the same source for both doubling and as local oscillator ensures a stable phase reference for the whole experiment. This latter feature is important here, since quantum state reconstruction involves phase-sensitive measurements.

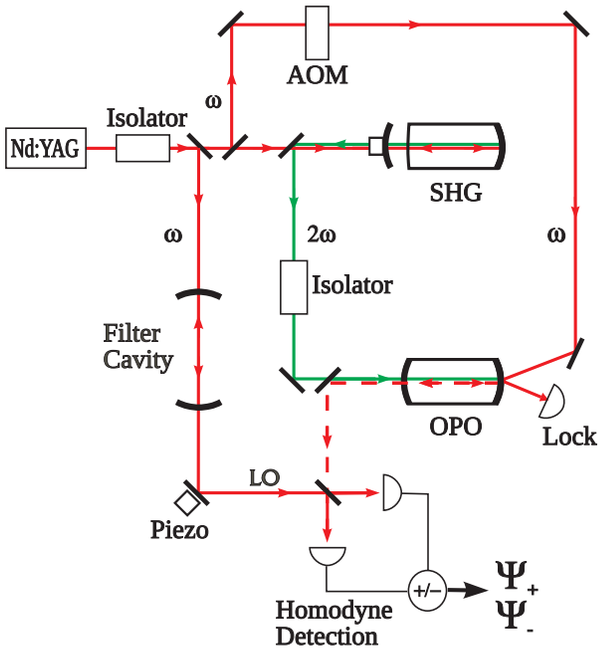

Figure 1: Experimental setup for the generation of squeezed vacuum states with a monolithic lithium niobate parametric oscillator (OPO). The hemilithic cavity (SHG) doubles the Nd:YAG laser which subsequently pumps the OPO. The local oscillator (LO) is combined with the signal beam at the homodyne detector.

2.1 Experimental Set-Up

A general overview of the set-up is shown in Fig.1. The laser source is a diode-pumped, continuous-wave Nd:YAG laser (Lightwave, model 122) with wavelength of λ= 1064 nm. The laser emits a single-frequency, 15 kHz linewidth, TEM_{00} wave whose frequency can be manually or electrically controlled. The free-running frequency stability is outstanding, with drifts of less than 10 MHz/min. Most of the laser power is used to pump an external frequency doubling cavity that efficiently doubles the laser frequency into green light at $\lambda = 532$ nm.[20]

The frequency doubler is a hemilithic standing-wave cavity formed by one curved mirror (the output coupler) and a nonlinear crystal (magnesium-oxide doped lithium niobate). One of the crystal faces is flat and the other is curved with a radius of curvature of 10 mm. The flat face is coated with an antireflection coating ($R < 0.1\%$) and the curved face is coated for high reflectivity at both 1064 and 532 nm. The faces perpendicular to the c-axis of the crystal are coated with gold for electrooptic modulation. The radius of curvature of the output coupler is 25 mm and it is coated for high transmission at 532 nm and 96% reflectivity at 1064 nm. The cavity is thus resonant at the fundamental frequency of the laser only, while the green light that is generated in each pass interferes constructively and exits through the output coupler.

The OPO also consists of a lithium-niobate crystal but is a monolithic 7.5 mm long standing-wave resonator. The crystal endfaces are polished spherically with 10 mm radii of curvature. One face is coated for high reflectivity at both 1064 and 532 nm, while the other face is the output coupler with transmissivity T= 2.1% at 1064 nm and high transmission at 532 nm. This crystal is also coated on two opposing sides with gold electrodes for electrooptic modulation. The fact that only the infrared light is resonant in the cavity simplifies the operation of this device. The green light double passes the resonator to enhance the nonlinear coupling, so that the threshold is reduced.

The temperature of the crystals in both doubler and OPO is actively controlled to a few millikelvin, at the phase-matching temperature of lithium-niobate (about 110°C). Due to the fact that standing-wave resonators are employed, two Faraday isolators are required in the set-up; the first to isolate the laser from the doubler and the second to isolate the doubler from the OPO.

The squeezed vacuum generated in the OPO is directed to a 50-50 beamsplitter and combined with a local oscillator for BHD. As was mentioned before, we used part of the original laser beam as the local oscillator. The laser beam was not injected directly into the beamsplitter, because the diode-pumped YAG laser has a large excess intensity noise at frequencies up to several MHz.[21] Given the fact that the spectrum of squeezing is best at frequencies of a few MHz, we used an optical filtering technique to suppress the excess noise. To this end, the laser beam passes through a high finesse cavity consisting of two high reflector mirrors spaced by 50 cm. The cavity with a bandwidth of 140 kHz acts in transmission as a low pass filter. An analysis of the noise of the local oscillator beam that is transmitted through the cavity shows that the excess noise of the laser is suppressed down to shot-noise for frequencies greater or equal to 1 MHz.[18]

The two photodetectors used for the BHD are Epitaxx ETX-500 photodiodes with removed window. We determined a quantum efficency of 97% for both photodiodes by calibrating their photocurrents with the incident laser power (measured by a thermopile from Laser Instrumentation). The photocurrents are processed by a low noise amplifier circuit with approximately flat gain up to 30 MHz. For a local oscillator power of 2 mW incident on one of the detectors, the electronic noise is sufficiently low. The shot-noise level at frequencies of a few MHz is 14 dB above the electronic noise level and still 5 dB above for frequencies around 24 MHz.

2.2 Experimental Procedure

The main steps of the experiment consist in stabilization of the cavity lengths, calibration of the BHD, and optimization of the mode-matching of the green beam to the OPO cavity mode for highest parametric gain.

The doubler cavity is actively stabilized by the Pound-Drever technique,[22] where the cavity crystal is modulated at 15 MHz and the ensuing amplitude modulation of the infrared beam is detected in transmission through the high reflector mirror by a fast photodetector. The error signal, generated by mixing the photocurrent with the modulating frequency, is fed back to the piezo of the cavity. We have also stabilized the laser frequency to the OPO cavity in a similar procedure as for the doubler, by injecting a weak 180 MHz frequency-shifted beam into the high reflector port of the OPO. But since both laser and OPO have good frequency stability and the OPO linewidth is high (2 , = 34 MHz), we have observed that it is possible to manually keep the laser frequency well in resonance during the time needed for data acquisition even without active stabilization.

The main steps for the calibration and performance of the BHD are the determination of the shot-noise level, of the noise suppression of the local oscillator, and of the beam overlap of the signal beam from the OPO with the local oscillator. The photocurrents from both detectors of the BHD are subtracted and added, resulting in the photocurrents i_- and i_+, respectively. The fluctuations of these photocurrents are then analyzed in a spectrum analyzer.

The shot-noise level is determined by comparing the fluctuations of the photocurrents i_- and i_+ when the open port of the beamsplitter (where later the signal from the OPO is injected) has vacuum input. The difference between these two photocurrents is within 0.3 dB for a wide range of frequencies. When the balancing of detector gains is optimized for a particular frequency, the accuracy is 0.2 dB.

The suppression of the local oscillator noise is checked by adding a strong amplitude modulation

to it, and measuring again the difference between the fluctuations of i_- and i_+. The suppression in our set-up is better than 20 dB.

The beam overlap of local oscillator and the signal from the OPO is an important factor, since it determines the homodyne efficiency of the BHD. To measure it, we inject a coherent beam at the high reflector port of the OPO. The transmitted beam interferes with the local oscillator at the beam splitter. A visibility of the interference fringes of more than 99% was reached, corresponding to near-perfect beam overlap.

The alignment and the mode-matching of the green pump to the OPO is optimized by operating the OPO above threshold as described in Ref.[23]. Further optimization of the pump alignment and the OPO temperature is done by measuring the parametric amplification of a small signal injected into the high reflector port of the cavity. With pump powers near the threshold power of the OPO (28 mW), classical parametric gain up to 3500 times was observed.

The last important parameter to check in the experimental scheme is the total detection efficiency. This involves the measurement of the escape efficiency of the OPO cavity, of the passive transmission loss from the OPO to the photodetectors, and, as mentioned above, of the homodyne (i.e., superposition) efficiency between the local oscillator and the signal light. The escape efficiency $\rho = T/(T + A)$, with T being the OPO output coupler transmission and A the total internal round trip loss, is not determined directly in our set-up because for monolithic resonators it is difficult to independently measure both A and T. Instead we measured the conversion efficiencies for resonant frequency doublingand for parametric down-conversion, where, in both cases, the maximum efficiency is equal to ρ. The measured values for maximum conversion efficiencies are 82% for frequency-doubling and 84% for down-conversion, which aftercorrection for imperfect mode-matching of the respective pump beams results in $\rho = 88\%$.[23, 20] The measured finesse of the OPO is 265, which, considering the free spectral range of 9 GHz, gives a linewidth 2 , =34 MHz (FWHM). The overall losses of propagation from the OPO to the photodetectors, due to absorption and scattering by mirrors, lenses and beamsplitter, are 2%.

In summary, the 99% homodyne, 98% propagation, 88% escape, and 97% detector quantum efficiencies lead to a total detection efficiency of η= 81% in our experiment. If we had perfect detection efficiency, the best degree of squeezing, limited by the escape efficiency only, would amount to 9.5 dB for this monolithic resonator.

3 Measurements of Squeezing

In this section, we show a series of mesurements that we have performed in order to characterize the squeezing from our monolithic resonator. We start with the direct mesurement of the squeezing and anti-squeezing spectra up to 30 MHz, followed by the measurement of both the variances and the distributions of the field fluctuations in phase space at a fixed analyzing frequency of 2 MHz.

3.1 The squeezing spectrum

The squeezed vacuum from the OPO is detected by measuring the fluctuations of the photocurrent i_- from the balanced homodyne detector. The resulting current is sent to a spectrum analyzer where the spectral density $\Psi_-(\Omega)$ is recorded. By choosing the local oscillator phase, we are able to record the fluctuations of the quadrature component $\hat{x}$ which corresponds to the maximum noise enhancement S_+ (antisquezing) and of the component $\hat{p}$ which corresponds to maximum noise reduction S_- (squeezing). For a given pump power P and analysis frequency Ω, the spectra are given by [24]

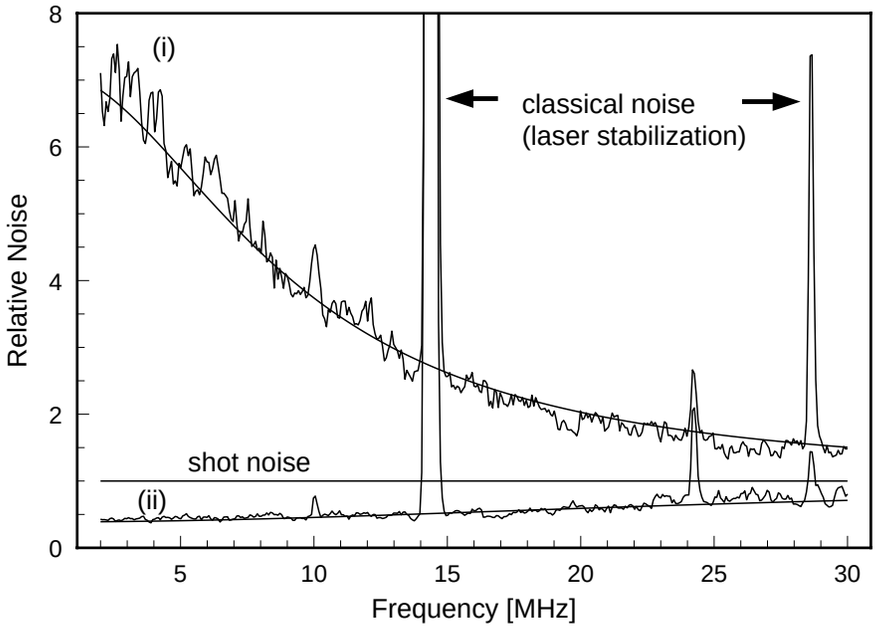

Figure 2: Spectral density Ψ_- as a function of the analysis frequency Ω. Trace (i) is the anti-squeezing spectrum and trace (ii) is the squeezing spectrum. The peak at 14.5 MHz and its harmonic come from the modulation of the doubling cavity used for the locking system. The resolution bandwidth for these measurements is 100 kHz, and the video bandwidth is 100 Hz.

$$S_{\pm}(\Omega, P) = \pm \frac{4\sqrt{P/P_{th}}}{(\Omega/\ ,\ )^2 + (1 \mp \sqrt{P/P_{th}})^2}, \tag{1}$$

where $\ ,\ = 17$ MHz is the cavity linewidth and $P_{th} = 28$ mW is the threshold power of the OPO. The noise $S_{\pm}$ relates to the actual measured values for the spectral densities Ψ_- by

$$\Psi_-(\Omega, P) = \Psi_0(1 + \eta S_{\pm}(\Omega, P)), \tag{2}$$

where Ψ_0 is the spectral density for a vacuum-state input to the BHD (obtained by blocking the output of the OPO), η is the total detection efficiency.

Since the photodetectors are broadband and calibrated from 1 to 30 MHz, we were able to record the whole spectrum of squeezing and antisqueezing by recording Ψ_- with the phase of the local oscillator fixed at either maximum or minimum noise levels. The electronic and shot-noise levels were also measured under the same conditions. After subtracting the electronic noise and normalizing the squeezing and antisqueezing to the shot noise level, with no further adjustments, we arrive at traces shown in Fig. 2. The theoretical predictions, plotted as solid lines, show good agreement with the experimental data and the independently measured detection efficiencies. Fig.2 also shows that there is still a reasonable amount of squeezing (about 3 dB) at high frequencies. The measurement at still higher frequencies was not possible due to the bandwidth of the photodetectors employed.

3.2 Squeezing and Fluctuation Statistics at a Fixed Frequency

As can be seen from the theoretical predictions for the squeezing spectrum (Eq. 1), the squeezing is best at low frequencies. Actually, for a lossless ($\eta = 0$) OPO at threshold (pump power $P = P_{th}$),

Figure 3: Spectral density $\Psi_-(\Omega = 2$ MHz) showing the fluctuations from the parametric amplifier as the phase of the local oscillator is scanned (trace i). The shot-noise level, obtained by blocking the squeezing is shown in trace ii. The squeezing level is 5.5 ± 0.2 dB.

perfect squeezing is predicted at frequency $\Omega = 0$. In our experiment, the technical noise in the detectors is very high at frequencies lower than 1 MHz. We have therefore chosen an analysis frequency far from any excess noise ($\Omega = 2$ MHz) to search for the best squeezing in our system.

The first step is the measurement of the photocurrent densities Ψ_- of squeezing as a function of the local oscillator phase. This data gives the variances of the quadrature phase amplitudes $\hat{x}_\theta = \hat{x}\cos\theta + \hat{p}\sin\theta$, and permits to understand how the quantum noise is distributed along the quadrature phase amplitudes of the field. Also, by invoking the fact that the squeezed vacuum generated by the OPO is a minimum uncertainty state, this measurement provides an accurate way to determine the total losses of the detection and compare them to the independent measurement. In Fig. 3 the spectral density of the photocurrent fluctuations $\Psi_-(\Omega =2$ MHz) for both squeezed vacuum (trace i) and normal vacuum (trace ii) states is shown. In order to determine more accurately the degree of squeezing at this frequency, we obtained $\Psi_-(\Omega = 2$ MHz) with the local oscillator phase kept at minimum noise level, i.e. maximum squeezing. The average over 400 points shows a squeezing degree of 5.5 ± 0.2 dB below the vacuum-noise level. The pump power for this measurement was approximately 3/4 of the threshold power.

The measurements shown in Figs. 2 and 3 determine Ψ_-, which can be translated into the variances of the quadrature amplitudes of the field. But more information about the state of the light field can be obtained by not only recording the variances, but the whole distribution $P_\theta(x_\theta)$ of the quadrature field fluctuations. As mentioned in the introduction, these distributions provide a way to determine the Wigner function and the density matrix of the quantum state.

The procedure we used to obtain the distributions $P_\theta(x_\theta)$ at several different phase angles in phase space consists in measuring the amplitude fluctuations of the photocurrent i_- from the BHD. This is done by recording the intermediate-frequency (IF) output of the spectrum analyzer on a digital oscilloscope (Nicolet 400), as the phase of the local oscillator is slowly scanned. Typical traces of the resulting photocurrent are shown in Fig. 4. The experimental conditions are the same as for the squeezing shown in Fig. 3.

The next step is to divide this 161,000 point trace corresponding to 79 different phase angles. For each phase angle, the photocurrent time trace was sorted into 128 bins. A total of 79 different histograms was thus obtained. As expected for the squeezed vacuum from the OPO, each of these histograms is a Gaussian, and corresponds, when normalized, to the Gaussian distribution of the a particular quadrature amplitude. The shot noise has also been recorded using the same procedure. Fig. 5 shows two of the 79 distributions, for the phase angles of maximum squeezing, and maximum antisqueezing, as well as that of the vacuum reference. More distributions are shown in the inset

Figure 4: Fluctuations of the photocurrent i_- at 2 MHz as the phase of the local oscillator is scanned. Left: Vacuum state, right: Squeezed vacuum state. The detection bandwidth is 100 kHz.

Figure 5: Probability distributions of the quadrature amplitude fluctuations at local oscillator phases corresponding to maximum squeezing and maximum anti-squeezing. The third distribution is obtained with normal vacuum. The solid lines are Gaussian fits. In the upper right corner, distributions for 11 different phase angles from 0 to π are shown.

of Fig.5.

4 Characterization of the Squeezed State

In Ref.[11] it has been shown that it is possible to reconstruct the Wigner function from a set of distribution functions $P_\theta(x_\theta)$, taken at angles θ between 0 to π. Thus, the measurements presented above provide the basis for a complete characterization of the quantum state. In addition to the determination of the Wigner function, it has been shown recently [14] that it is possible to determine the density matrix and the photon number distributions directly from the set of distributions $P_\theta(x_\theta)$.

In the following, we discuss the procedure for the reconstruction of both Wigner function and density matrix for the squeezed vacuum state, and in particular its photon number distribution.

4.1 Determination of the Wigner function

The Wigner function is a quasi-probability distribution in phase space, differing from a classical distribution mainly because it can be negative and cannot be measured directly, since it is a joint distribution of the eigenvalues of two noncommuting observables. What is measurable though, are the marginal distributions $P_\theta(x_\theta)$, which are positive definite probability distributions. These distributions are directly related to the Wigner distribution $W(x,p)$ through the relation [11]

$$P_\theta(x_\theta) = \int_{-\infty}^{\infty} W(x_\theta \cos\theta - p_\theta \sin\theta, x_\theta \sin\theta + p_\theta \cos\theta) dp_\theta, \tag{3}$$

where $p_\theta = x_{\theta+\pi/2} = -x\sin\theta + p\cos\theta$, and θ is the angle of rotation in the x,p-phase space.

Using the distributions $P_\theta(x_\theta)$ obtained experimentally, the Wigner function can be reconstructed by inverting the above equation. This inversion involves the so-called inverse Radon transformation. The reconstructions of states using this technique has been termed *optical homodyne tomography* by Smithey et al. in Ref.[12].

For a squeezed vacuum state of the electromagnetic field mode with frequency Ω, the Wigner function is given by

$$W_{sq}(x,p) = \frac{\exp\left[-\frac{1}{2}\left(\frac{x^2}{1+\eta S_+(\Omega)} + \frac{p^2}{1+\eta S_-(\Omega)}\right)\right]}{2\pi\sqrt{(1+\eta S_+(\Omega))(1+\eta S_-(\Omega))}} \ .$$

The inversion algorithm used for the determination of the Wigner function consists in a convolution of the measured histograms with a particular filter function (filtered back-projection). The resulting Wigner functions for the vacuum and the squeezed vacuum state and their contour lines are shown in Fig. 6. We remark that no corrections for detection and escape efficiency were made. The numerical error of this reconstruction is estimated to be less than 2%. An analysis of the ratio of the two halfwidths of the contour lines of the Wigner function of the squeezed vacuum state at $x = p = 0$ shows good agreement with the directly observed variances of the squeezing (5.5 dB) and anti-squeezing (12 dB) shown in the previous section.[18]

4.2 Determination of the Density Matrix and Photon-Number Distribution

In addition to the Wigner distribution, it is also possible to determine the density matrix in the Fock basis of the radiation field directly from the data, without any filtering (smoothing).[13] The

Figure 6: Wigner function and its contours (a) of a vacuum state, (b) of a squeezed vacuum state.

elements of the density matrix ρ_{nm} are related to the distributions by

$$\rho_{nm} = \int_0^{\pi} \int_{-\infty}^{+\infty} P_\theta(x_\theta) f_{nm}(x_\theta) e^{i(n-m)\theta} dx_\theta d\theta, \tag{4}$$

where f_{nm} are transcendental functions given in Refs.[15, 25].

Carrying out the integration for the set of measured distributions $P_\theta(x_\theta)$ we obtained the elements of the density matrix ρ in the Fock basis for the squeezed vacuum state of our experiment.[26] Of particular interest are the diagonal elements ρ_{nn}, which give the photon number distribution of the state. From Eq.4, these are obtained from the angle-averaged probability distributions $P(\bar{x}) = \int P(x_\theta) d\theta / 2\pi$.[27] According to Ref.[28], for the photon-number distribution of an ideal squeezed vacuum state zeroes for the probabilities of odd photon numbers are predicted. For the experimentally generated squeezing, the various losses that occurred inside the resonator, during propagation and in the detection lead to a state that is not of minimum uncertainty, but mixed. For such a state, the photon number distribution is given by [29]

$$\rho_{nn} = 2\sqrt{\frac{(2+\eta S_-)(1+S_-)}{2+2S_--\eta S_-}} (\eta s)^n P_n^+((1-\eta)s), \tag{5}$$

with $s = |S_-|/\sqrt{4+4S_-+2\eta S_-^2-\eta^2 S_-^2}$. $P_n^+(t)$ is the nth Legendre polynomial with positive coefficients, which in terms of the usual Legendre polynomial P_n can be written as $P_n^+(t) = (-i)^n P_n(it)$. The probabilities for the odd photon numbers are nonzero, but for small loss, high detection efficiencies and strong squeezing the distribution still exhibits oscillations. In Fig. 7 we present the photon number distribution derived from measured data together with the predicted distribution given by Eq.5, showing good agreement.

Figure 7: Photon-number distributions reconstructed from the set of quadrature amplitude distributions $P_\theta(x_\theta)$. The left picture shows the photon number distribution of a vacuum state, the right one that of a squeezed vacuum state. The points refer to experimental data and the histograms to theoretical predictions.

5 Conclusions

An optical parametric amplifier has been used to generate squeezed states of light, which, combined with the technology of monolithic resonators, resulted in a compact and stable device. Given that the length of these resonators is short, the spectrum of squeezing is broader than for most discrete cavities. We have been able to record the squeezing and anti-squeezing spectra up to 30 MHz. The highest measured degree of squeezing was 5.5 dB at a frequency of 2 MHz.

In addition, we have applied optical homodyne tomography to characterize states of the light field. For the first time, the Wigner function of a highly squeezed state in the continuous regime and the density matrix in the Fock basis were reconstructed. Due to the high degree of squeezing and relatively high detection efficiency, oscillations in the photon number were observed for the first time. The determination of the density matrix of the squeezed light shows the practical applicability of homodyne detection combined with novel reconstruction techniques to obtain complete information about a quantum state. In particular, with the determination of the photon statistics, we have demonstrated that this technique is a very powerful alternative to photon counting.

We wish to acknowledge colleagues that participated with their ideas and their hands to make this experiment possible: T. Müller, J.-Ph. Poizat, R. Paschotta, and A. White. We thank M. G. Raymer, A. Faridani, and D.F. McAlister for providing us with a program for the inverse Radon transform, and U. Janicke for improvements regarding the numerical inversion. We also acknowledge U. Leonhardt for several discussions about the complete characterization of a quantum state. S. F. Pereira was supported by the Humboldt Foundation. Financial support for this work was provided by the Deutsche Forchungsgemeinschaft, ESPRIT Project BRA 6934 - QUINTEC and the EC Network "Non-classical Light".

REFERENCES

1. Z. Y. Ou and L. Mandel, Phys. Rev. Lett. **61**, 50 (1988);

2. Z. Y. Ou, S. F. Pereira, H. J. Kimble, and K. C. Peng, Phys. Rev. Lett. **68**, 3663 (1992);

3. L. A. Wu, M. Xiao, and H. J. Kimble, J. Opt. Soc. of Am. B **4**, 1465 (1987);

4. K. Bencheikh, J. A. Levenson, Ph. Grangier, and O. Lopez, Phys. Rev. Lett. **75**, 3422 (1995).

5. M. Xiao, L. A. Wu, and H. J. Kimble, Phys. Rev. Lett. **59**, 278 (1987).

6. E. S. Polzik, J. Carri, and H. J. Kimble, Phys. Rev. Lett. **68**, 3020 (1992).

7. Z. Y. Ou, S. F. Pereira, and H. J. Kimble, Phys. Rev. Lett. **70**, 3229 (1993).

8. J. A. Levenson, I. Abram, T. Rivera, P. Fayolle, J. C. Garreau, and P. Grangier, Phys. Rev. Lett. **70**, 267 (1993).

9. S. Schiller et al., in preparation.

10. H. P. Yuen and V. W. S. Chen, Opt. Lett. **18**, 177 (1983); B. Schumacher, Opt. Lett. **19**, 189 (1984).

11. K. Vogel and H. Risken, Phys. Rev. **A40**, 2847 (1989).

12. D. T. Smithey, M. Beck, M.G. Raymer, A. Faridani, Phys. Rev. Lett. **70**, 1244 (1993)

13. G. M. D'Ariano, C. Macchiavello, and M. G. A. Paris, Phys. Rev. **A50**, 4298 (1994).

14. G. M. D'Ariano, U. Leonhardt, and H. Paul, Phys. Rev. **A52**, R1801 (1995).

15. U. Leonhardt and H. Paul, and G. M. D'Ariano, Phys. Rev. **A52**, 4899 (1995).

16. M. Koashi, K. Kono, T. Hirano, and M. Matsuoka, Phys. Rev. Lett. **71**, 1164 (1993).

17. W.J. Kozlovsky, C.D. Nabors, R.C. Eckardt, and R.L. Byer, Opt. Lett. **14**, 66 (1989).

18. G. Breitenbach, T. Müller, S. F. Pereira, J. Ph. Poizat, S. Schiller, and J. Mlynek, J. Opt. Soc. Am. B **12**, 2304 (1995).

19. R. E. Slusher, P. Grangier, A. LaPorta, B. Yurke, and M. J. Potasek, Phys. Rev. Lett. **59**, 2566 (1987); T. Hirano and M. Matsuoka, Opt. Lett. **15**, 1153 (1990); C. Kim and P. Kumar, Phys. Rev. Lett. **73**, 1605 (1994).

20. R. Paschotta, K. Fiedler, P. Kürz, R. Henking, S. Schiller, and J. Mlynek, Opt. Lett. **19**, 1325 (1994)

21. T. J. Kane, IEEE Phot. Tech. Lett. **2**, 244 (1990).

22. R. Drever, J. Hall, F. Kowalski, J. Hough, G. Ford, A. Munley, and H. Ward, Appl. Phys. B **31**, 97 (1983).

23. G. Breitenbach, S. Schiller, J. Mlynek, J. Opt. Soc. Am. B **12**, 2095 (1995).

24. M. J. Collett and D. F. Walls, Phys. Rev. **A32**, 2887 (1985)

25. U. Leonhardt, M. Munroe, T. Kiss, Th. Richter, and M. G. Raymer, Opt. Commun. (submitted).

26. S. Schiller, G. Breitenbach, S. F. Pereira, T. Müller, and J. Mlynek, in preparation.

27. M. Munroe, D. Boggavarapu, M. E. Anderson, and M. G. Raymer, Phys. Rev. **A52**, R924 (1995).

28. W. Schleich and J. Wheeler, J. Opt. Soc. Am. B **4**, 1715 (1987).

29. The photon distribution can be derived from

$$\rho_{nn} = \int\int dpdx W_{sq}(x,p) W_n(x,p), \tag{6}$$

where W_n and W_{sq} are the Wigner functions for the Fock state $|n\rangle$ and squeezed state, respectively. The integral is evaluated using generating functions for the Laguerre and Legendre polynomials in the series $\Sigma\rho_{nn}z^n$.